Effect of texture randomization on the slip and interfacial robustness in turbulent flows over superhydrophobic surfaces

Jongmin Seo and Ali Mani

Phys. Rev. Fluids **3**, 044601 — Published 2 April 2018

DOI: 10.1103/PhysRevFluids.3.044601

Effect of texture randomization on the slip and interfacial robustness in turbulent flows over superhydrophobic surfaces

Jongmin Seo and Ali Mani
Center for Turbulence Research, Stanford University, Stanford, California 94305, USA

Superhydrophobic surfaces demonstrate promising potential for skin friction reduction in naval and hydrodynamic applications. Recent developments of superhydrophobic surfaces aiming for scalable applications use random distribution of roughness, such as spray coating and etched process. However, most of previous analyses of the interaction between flows and superhydrophobic surfaces studied periodic geometries that are economically feasible only in lab-scale experiments. In order to assess the drag reduction effectiveness as well as interfacial robustness of superhydrophobic surfaces with randomly distributed textures, we conduct direct numerical simulations of turbulent flows over randomly patterned interfaces considering a range of texture widths $w^+ \approx 4 - 26$, and solid fractions $\phi_s = 11\%$ to 25%. Slip and no-slip boundary conditions are implemented in a pattern, modeling the presence of gas-liquid interfaces and solid elements. Our results indicate that slip of randomly distributed textures under turbulent flows are about 30% less than those of surfaces with aligned features of the same size. In the small texture size limit $w^+ \approx 4$, the slip length of the randomly distributed textures in turbulent flows is well described by a previously introduced Stokes flow solution of randomly distributed shear-free holes. By comparing DNS results for patterned slip and no-slip boundary against the corresponding homogenized slip length boundary conditions, we show that turbulent flows over randomly distributed posts can be represented by an isotropic slip length in streamwise and spanwise direction. The average pressure fluctuation on gas pocket is similar to that of the aligned features with the same texture size and gas fraction, but the maximum interface deformation at the leading edge of the roughness element is about twice larger when the textures are randomly distributed. The presented analyses provide insights on implications of texture randomness on drag reduction performance and robustness of superhydrophobic surfaces.

I. INTRODUCTION

Superhydrophobic surfaces(SHSs) are non-wetting surfaces consisting of hydrophobic chemical coating and micro-nano scale structures that lead to extremely high macroscopic contact angle ($\gtrapprox 150^\circ$) and small contact angle hysteresis [1, 2]. When submerged in liquid, micro-structures on SHSs can hold gas pockets which replace the contact area of liquid to solid elements with liquid to gas, causing slippage effect. The macroscopic effect of slippage from bubble mattress has been demonstrated significantly reducing skin friction up to about 20% in laminar flows [3]. In laminar flows, theoretical investigations of the flow and slippage behavior, depending on the geometric parameters, have been established for the regularly arranged SHSs [4–6], and validated [7]. A shear-driven drainage mechanism of failure of slippery surfaces has been studied [8, 9] and a remedy for the shear-driven drainage has been proposed [10]. A great deal of experimental research aimed to test the skin friction reduction effect of SHS in regimes relevant to realistic scenarios, where the overlying flow is turbulent [11–16].

The physical understanding as well as predictions of kinematics of turbulent flows over SHSs have been established by direct numerical simulations (DNSs) of the turbulent channel flows. In DNSs, SHSs are modeled as a surface with a single slip length [17–19], an idealized air layer with finite thickness [20], or patterned slip and no-slip boundaries [21–30]. Effects of slip on turbulent flow have been first investigated by Min and Kim[17]. By conducting DNS of turbulent flows over prescribed, single slip length, Min and Kim[17] showed that the streamwise slip contributes to the upward shift of the whole mean velocity profile by slip velocity in wall unit, b^+, and showed that any finite spanwise slip, b_z^+, causes downward shift of the outer layer, ΔU^+, due to shrinkage of the buffer layer. Fukagata *et al.*[18] suggested a phenomenological model for estimation of drag reduction combining effects of streamwise and spanwise slip in a modified form of the log-law. Park *et al.*[22] conducted DNS of turbulent flows over SHS streamwise ridges for a wide range of texture size and Reynolds numbers and showed that the key parameter determining drag reduction (DR) is b^+. Seo and Mani [28] presented a prediction law for slip length outside of Stokes flow regime as a function of design and flow parameters as $b^+ \sim {L^+}^{1/3}/\sqrt{\phi_s}$, where L^+ is texture periodicity in wall unit and $\phi_s = A_{\text{solid}}/A_{\text{total}}$ is solid fraction of the textured surface. The prediction for slip length suggested by [28] is applied to liquid-infused surfaces and their validity is investigated in [31]. Alongside kinematics of SHS in turbulent flows, the mechanisms leading to loss of gas pockets, thus to drag increase, have been studied by Seo *et al.*[27] when the gas-liquid interface responds to the pressure fluctuations from overlying turbulent flows. They identified a mechanism of bubble depletion that caused by stagnation of slipping flows at the leading edge of solid roughness elements. Seo *et al.*[32] presented an additional breakup mechanism of gas pockets by flow induced capillary waves, when the gas-liquid interfaces dynamically interact with a turbulent flow. The deleterious effect of increasing texture size on the drag observed by these DNS studies is

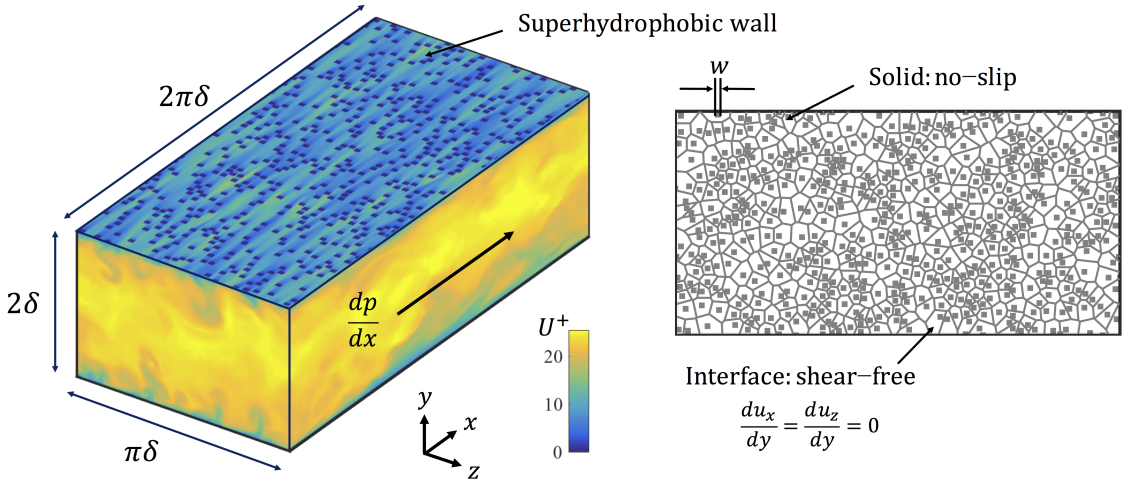

Figure 1. An illustration of periodic turbulent channel with superhydrophobic walls. An instantaneous snapshot of streamwise velocity is plotted. A Voronoi decomposition of surface around textures is shown.

qualitatively consistent with theoretical analysis [33], and experimental investigations [13, 15, 34]. Recently Ling et al. [16] studied the mechanism of bubble depletion due to saturation in turbulent boundary layer experiments.

Particularly in economically scalable methods for mass production of SHS, randomly distributed roughness structures are the relevant option in practice [13–15, 35–37]. In a Stokes flow regime, the relation of slip length to texture size and solid fraction for randomly distributed SHS was first established, analytically by Sbragaglia and Prosperetti [38]. They suggested a heuristic slip length, b, in terms of a shear-free hole diameter, a, and solid area fraction, ϕ_s,

$$b = \frac{8}{9\pi}\frac{(1-\phi_s)}{\phi_s}a, \quad \phi_s \to 0. \tag{1}$$

Samaha *et al.*[39] conducted laminar flow simulations over SHS with randomly distributed textures and showed converged results with different replicas of random distribution of textures for fixed texture size and solid fraction. Samaha *et al.*[39] found that Sbragaglia and Prosperetti's solution is valid for a range of solid fraction $0.1 \leq \phi_s \leq 0.5$. Bidkar *et al.*[13] and Ling *et al.*[15] showed that the non-dimensional surface roughness in wall unit, k^+, was needed to be significantly smaller than the viscous sublayer to obtain successful drag reduction. Previous investigations of turbulent flows over SHS with randomly distributed texture are experimental [13–15], while analyses from above-mentioned DNSs only considered geometries with regularly aligned textures. DNS of turbulent flows over randomly textured SHS is beginning to emerge from some of the recent studies [40]. Systematic investigations of texture randomization in DNS can augment quantitative understanding of turbulent flows over the randomly distributed texture.

In this paper, we investigate the effects of texture randomness in SHS on engineering-level performance when overlaid with a turbulent flow. This study aims to establish the quantitative estimates of drag reduction and interfacial robustness in regimes relevant to practical applications. We explore both kinematic properties as well as pressure loads from DNS data, and the results are compared with SHSs that have the same features but organized in a structured fashion. We will discuss design implications of texture randomness by quantifying performance degradation both in terms of drag reduction and robustness.

II. MODELING AND SIMULATION

A. Governing equations and boundary conditions

We numerically solve the incompressible Navier–Stokes equations for turbulent liquid flows,

$$\nabla \cdot \vec{u} = 0, \tag{2}$$

$$\frac{\partial \vec{u}}{\partial t} + \vec{u} \cdot \nabla \vec{u} = -\frac{1}{\rho}\nabla p + \nu \nabla^2 \vec{u}, \tag{3}$$

in the periodic channel, where $\vec{u}$ is velocity fields, p is liquid pressure, ν is the kinematic viscosity and ρ is density of liquid.

The channel has top and bottom walls treated with superhydrophobic surfaces consisting of solid roughness elements that entrap gas pockets. The solid-liquid boundary is described by no-slip condition and the gas-liquid interface is treated as shear-free boundary condition as shown in figure 1. The shear-free boundary condition on the gas-liquid interface is an idealized condition, but is shown to be acceptable for gas-liquid systems involving low viscosity ratios [41]. The solid roughness elements are randomly distributed over the surface. In current simulations, we do not include the dynamic coupling of the deformation of gas-liquid interface with overlying flows. Instead we consider interface deformation in a post-processing method presented by Seo *et al.*[27], using the wall pressure fields from DNS data. In our analysis, the interface height, η, measured from the tip of textures ($y = 0$), is quantified solving the linearized Young-Laplace equation,

$$\sigma \nabla^2 \eta \approx \Delta P, \tag{4}$$

where σ is the surface tension and ΔP is the pressure difference across the interface, $P_{\text{liquid}} - P_{\text{gas}}$. As in Seo *et al.*[27], we assumed the pressure in the gas layer is homogeneous and the mass of the gas is conserved, $\iint \eta \, \mathrm{d}x \, \mathrm{d}z = 0$.

B. Dimensionless physical parameters

In our computational modeling, we consider four dimensionless parameters relevant to turbulence, superhydrophobic surfaces and gas-liquid interface. The first parameter is the friction Reynolds-number, $\mathrm{Re}_\tau = u_\tau \delta/\nu$, which is Reynolds number based on friction velocity $u_\tau = \sqrt{\tau_w/\rho}$, where τ_w is wall shear, and the boundary layer thickness, δ, equal to channel half height. In Seo *et al.*[27], the effects of SHS on turbulent flows is shown to be insensitive to the Reynolds number, as long as all other parameters are kept constant when normalized by flow inner scale. Guided by these results, in the current study we use $\mathrm{Re}_\tau = 197.5$ in our simulations.

The second parameter is the width of the texture in viscous unit, $w^+ = w\delta/\nu = w/\delta_\nu$. The size of texture characterizes the drag reduction when the solid fraction is fixed for periodically aligned textures [22, 25, 28]. In the present work, we have investigated textures with width $w^+ \approx 4 - 26$. We aim to match the smallest texture width $w^+ \approx 4$ to that of real superhydrophobic surfaces with texture sizes of $\sim O(10)\mu m$, considering the δ_ν in realistic turbulent boundary layer is $\sim O(1)\mu m$.

Another, texture-related dimensionless parameter is the solid fraction, ϕ_s. A typical range of ϕ_s is $10\% - 20\%$ and does not vary by order of magnitude [13–15]. In the present study we considered $\phi_s = 1/9, 1/6$, and $1/4$.

For superhydrophobic surfaces aligned geometries, the texture periodicity is given by combination of texture width and gas fraction, for example $L^+ = w^+/\sqrt{\phi_s}$ for isotropic posts [27, 28] or $L^+ = w^+/\phi_s$ for streamwise ridges. Since there is no periodicity in our random texture geometry, we define a nominal texture size $L_n^+ = w^+/\sqrt{\phi_s}$, to compare results with aligned posts.

The last dimensionless parameter is Weber number $We^+ = \rho u_\tau^2 \delta_\nu/\sigma$. The Weber number can characterize the interfacial robustness in which the momentum from turbulence competes against the surface tension. In our analysis on the interfacial robustness we use $We^+ = 10^{-3} - 10^{-2}$, corresponding to a practical application with a typical boundary layer [27].

C. Numerical details

The three-dimensional Navier-Stokes equations are numerically solved with the code of Seo *et al.*[27] using a second-order finite-difference method on a staggered mesh. The channel size and number of grid points are described in table I. Independence of turbulence statistics on size of domain is well verified [27]. The minimum number of grid per texture width is kept the same as in [27] which has been shown to produce grid independent turbulence statistics against the resolution test case with twice number of grid per texture.

In addition to the patterned slip and no-slip simulations, we conducted DNS over homogenized slip surfaces with a uniform, isotropic slip length, b^+ as used in Min and Kim[17]. The DNSs with homogenized slip model use the slip lengths obtained from DNS of flows over surfaces with patterned boundary conditions. In the homogenized simulations, number of grid points is down to $192(x) \times 192(z) \times 128(y)$. The fractional-time advancement scheme uses the second-order Adams-Bashforth scheme for the non-linear and wall-parallel diffusion terms, and the second-order Crank-Nicholson scheme for the wall-normal diffusion terms [42]. The simulations were run for at least $35\delta/u_\tau$ and only the snapshots after $t = 10\delta/u_\tau$ were used for statistical sampling to exclude the initial transient signals. The flow is driven by a time-constant mean pressure gradient to ensure the pre-specified w^+.

Case	w^+	ϕ_s	L_n^+	Re_τ	D_x^+	D_z^+	$N_x \times N_z \times N_y$	U_s^+
R04ϕ_{s25}	4.3	1/4	8.6	197.5	1240.9	620.5	1152 × 576 × 128	1.6
R04ϕ_{s16}	4.3	1/6	10.5	197.5	1240.9	620.5	1152 × 576 × 128	2.8
R04$_{1,2}$	4.3	1/9	12.9	197.5	1240.9	620.5	1152 × 576 × 128	4.5
R08	8.6	1/9	25.8	197.5	1240.9	620.5	576 × 288 × 128	6.3
R13	12.9	1/9	38.7	197.5	1240.9	620.5	384 × 192 × 128	7.6
R26$_{1,2,3,4}$	25.8	1/9	77.4	197.5	1240.9	620.5	384 × 192 × 128	10.9
H04	$b^+ = b_z^+ = 4.5$			197.5	1240.9	620.5	192 × 192 × 128	4.5
H26	$b^+ = b_z^+ = 10.9$			197.5	1240.9	620.5	192 × 192 × 128	10.9

Table I. Simulation parameters. w^+ is the texture width, ϕ_s is solid area fraction, and Re_τ is the friction Reynolds-number. L_n^+ is a nominal texture size, $L_n^+ = w^+/\sqrt{\phi_s}$. Domain size in viscous unit is D_x^+ and D_z^+ for streamwise and spanwise directions. U_s^+ is the slip velocity in wall unit. Note that $b^+ = U_s^+$ by definition, $u_s = b\frac{dU}{dy}|_{wall}$. The number of grid points are N_x, N_z, and N_y, for streamwise, spanwise, and wall-normal directions respectively. Subscripts represent the replicated cases with different texture arrangements for the same texture parameters.

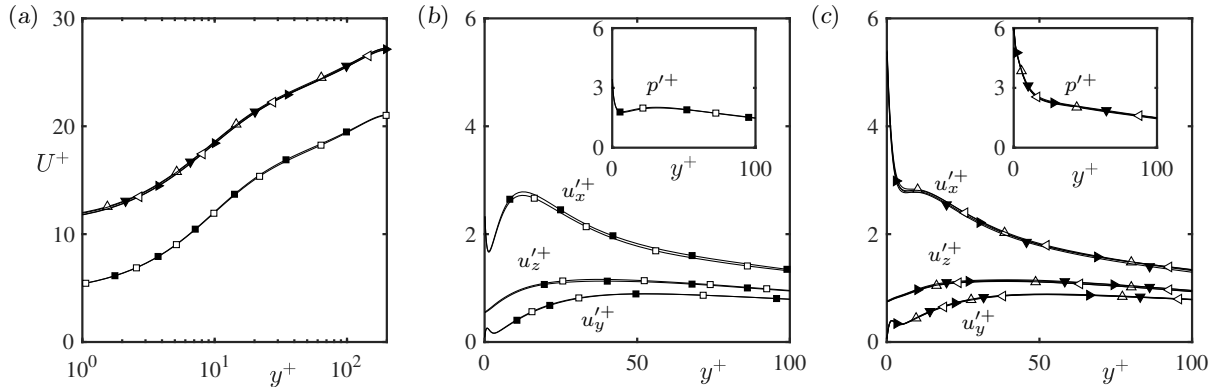

Figure 2. Turbulence statistics with different post arrangements with $\phi_s = 1/9$ at $Re_\tau \approx 200$. (a) Mean streamwise velocity profile; (b) $w^+ \approx 4$, rms velocity and pressure fluctuations; (c) $w^+ \approx 26$, rms velocity and pressure fluctuations. -■-, R04$_1$; -□-, R04$_2$; -▼-, R26$_1$; -△-, R26$_2$; -►-, R26$_3$; -◁-, R26$_4$.

D. Texture arrangement and repeatability of statistics

We randomly distribute posts in the computational domain and avoid overlapping using the algorithm used by Samaha *et al.*[39]. Specifically, the i'th post is located randomly in the domain then if any of distance $r_{ij} = \sqrt{r_i - r_j}, j = (1, 2, ...i-1)$, is less than $2\sqrt{2}w$, the allocation of the post is ignored and a new random location is tested. In this notation, $r_i = (x_i, z_i)$ is the location of i'th number of post, and r_j is the positions of other posts assigned before the i'th post. This procedure is repeated until the total number of posts matches the targeted solid fraction.

To assess the variability of results due to different random ensembles, we consider multiple realizations of random textures formed by the same texture parameters, w^+ and ϕ_s. Two replicas for $w^+ \approx 4$ and $\phi_s = 1/9$ are generated and all statistically averaged flow quantities (e.g. mean velocity profile, turbulence intensities) from the two samples collapse within 2% difference as shown in figure 2. Likewise, we additionally examine the repeatability of the statistics for larger textures with $w^+ \approx 26$. Four replicas are generated with different texture arrangements. Turbulent statistics show that all different texture arrangements produce results within 3% difference throughout the channel as shown in figure 2. This implies that our domain had sufficiently large areas for statistically converged mean friction, even when a single realization of these surfaces is used.

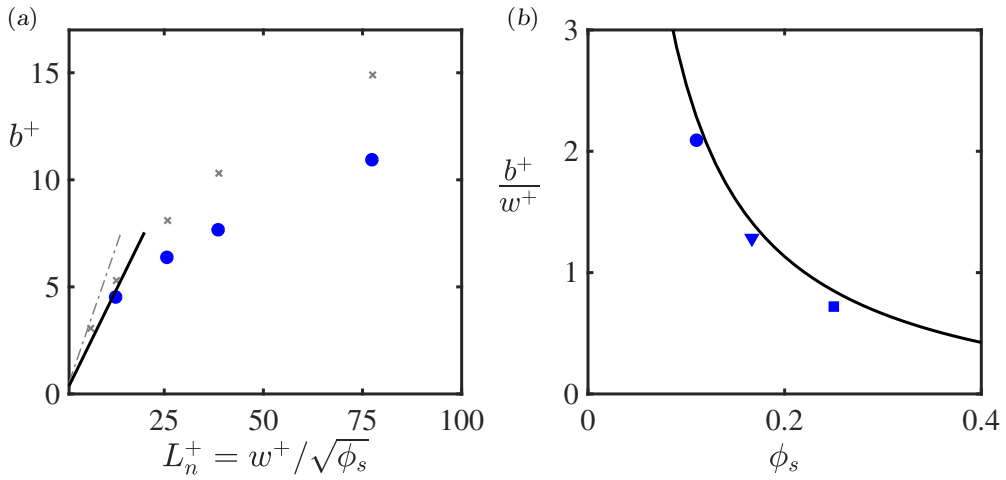

Figure 3. (a) Slip length, b^+, versus texture size, $L_n^+ = w^+/\sqrt{\phi_s}$, with $\phi_s = 1/9$. Symbols are DNS solutions; ●: randomly distributed posts, ×: aligned posts [28]. Lines are Stokes flow solutions; ——: Equation (1) by [38]; – · – · –: Ybert *et al.*[5] (*b*) Slip length, b^+, normalized by texture width, w^+, versus solid fraction, ϕ_s, at $w^+ \approx 4$. ●: R04$_1$, ▼: R04ϕ_{s16}, ■: R04ϕ_{s25}, ——: [38]

III. RESULTS AND DISCUSSION

A. Slip length

We first analyze the impact of geometric randomness on slip length as compared to that of aligned posts. For each geometric configuration, we fix $L_n^+ = w^+/\sqrt{\phi_s}$ (as well as w^+). The slip lengths of randomly distributed SHS textures with widths $w^+ \approx 4-26$, and a fixed solid fraction $\phi_s = 1/9$, is plotted in terms of effective texture size in figure 3(*a*). In the small texture size limit, the slip length from the DNS data matches with the heuristic model by Sbragaglia and Prosperetti [38]. The validity limit of Stokes flow solution is up to $L_n^+ \approx 13$ for the randomly distributed post case, while the validity of Stokes flow solution for the aligned post case was limited up to $L_n^+ \approx 10$. Figure 3(*b*) shows that for $w^+ \approx 4$ the dependence on ϕ_s matches the Stokes flow prediction by Sbragaglia and Prosperetti [38]. In the large effective texture size limit, the slip length increases non-linearly as previously observed for periodic geometries [28]. In comparison with the DNS data from aligned posts, the randomly distributed posts produce approximately 30% less slip length for the same nominal texture size L_n^+.

The deterioration of slip length in the case of randomly distributed posts can be best understood by observation of the streamwise velocity contours in figure 4. When the posts are perfectly aligned, the shear free regions are connected as in the case of streamwise ridges. As shown in figure 4, this leads to presence of fast streaks near the wall. Since these streaks are not interrupted by the geometry, they can persist for a long length scale on the order of $O(10^2)\delta_\nu$. However, the random arrangement of posts leads to a finite slipping area in streamwise direction, halted by another post. Therefore the net effect of local slip (i.e. slip length) is thus reduced in the randomly distributed posts compared to aligned posts.

B. Turbulence statistics

We compare the mean velocity profiles obtained from simulations of homogenized isotropic slip length models and that of the corresponding DNS of randomly distributed posts in figure 5(*a*). The mean velocity profile from homogenized slip simulation with isotropic slip length matches well with that from patterned slip DNS in the entire channel. The modification of mean velocity profiles for SHSs due to shrinkage of the buffer layer is measured by calculating the velocity deficit $\Delta U^+ = U_{b,smooth} - (U_{b,SHS} - b^+)$ at the outermost location from the wall, $y = \delta$ as shown in figure 5(*b*). The excellent match of the velocity profile of homogenized model with that of patterned slip and no-slip DNS implies that the estimation of $\Delta U^+(b^+)$ from isotropic slip length model, such as $\Delta U^+ = 4 - (1 - (4/(4 + b_z^+))$ in Busse and Sandham[19], can be used to predict drag reduction for SHS with randomly distributed texture. The validity of homogenized isotropic slip length model covers a wide range of texture size up to $L_n^+ \approx 77$. In contrast, for surfaces with aligned textures a previous analysis by Seo and Mani [28] showed that the the validity is limited to

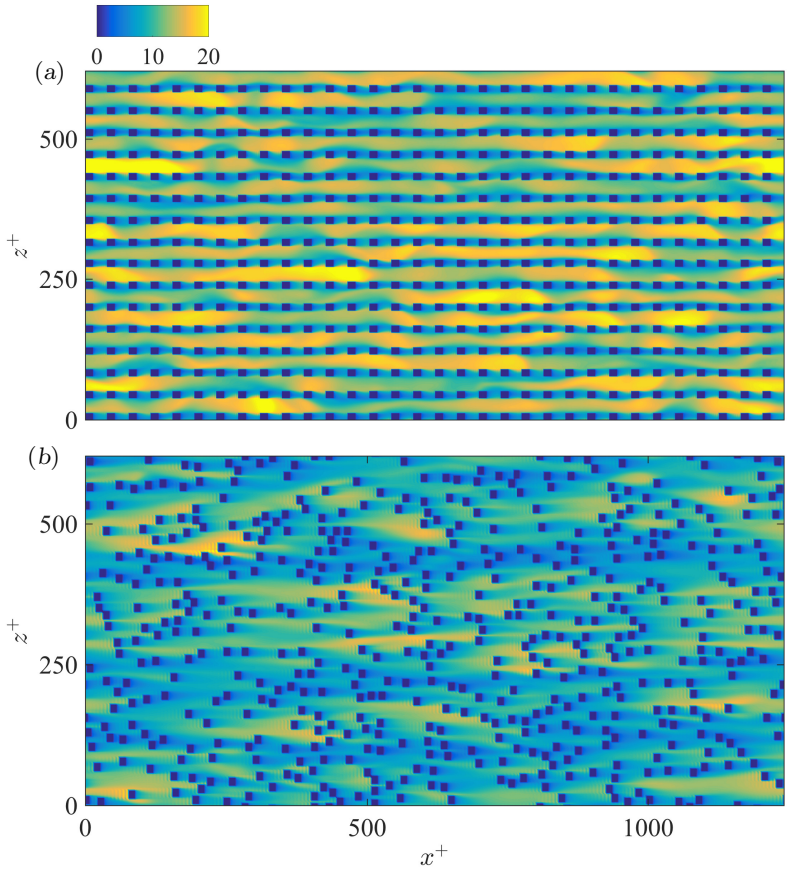

Figure 4. Instantaneous streamwise velocity contours at $y^+ = 0$ for $L_n^+ \approx 38.7$: (a) aligned posts (b) randomly distributed posts.

texture size of $L_n^+ \lesssim 10$.

The turbulence fluctuation term, $q'(x, y, z, t)$, is decomposed into one signal associated with spatially coherent fluctuation $\tilde{q}(x, y, z)$ and random signal $q''(x, y, z, t)$

$$q'(x, z, y, t) = \tilde{q}(x, z, y) + q''(x, z, y, t), \tag{5}$$

where q represents variables $(u_x, u_y, u_z; p)$. This decomposition is used in many DNS of turbulent flows over periodic geometries with a finite wavelength [23–25, 27]. Since there is no periodic unit in our current study, we use the Voronoi diagram to define the unit area surrounding each post. For example, a Voronoi diagram for RP38 case is shown in figure 1. We denote $\tilde{q}$ as a quantity that is averaged in time, then ensemble averaged over all different post locations using the Voronoi area.

Turbulence statistics for velocity and pressure fluctuations are summarized in figure 6. For comparison we plot two simulations with the smallest, $L_n^+ \approx 12.9$ (R04), and the largest texture size, $L_n^+ \approx 77.4$ (R26), accompanied by homogenized simulations provided with the same slip lengths of the two patterned surfaces (H04, H26), and a smooth wall. In $L_n^+ \approx 12.9$, near wall velocity fluctuations of flows over randomly distributed posts are intensified, compared to the smooth wall. The intensification of turbulence contribution q'' near the wall is well captured by the homogenized slip length simulation. Therefore the intensification of q'' near wall is due to the increase of slip, while $\tilde{q}$ is induced by the pattern-induced velocity and pressure fluctuations. Away from the wall ($y^+ \gtrapprox 50$), the near wall fluctuations are diminished and all fluctuations merge to a smooth wall profile. The contribution of coherent fluctuation $\tilde{q}$ to the total fluctuation become larger when texture size is $L_n^+ \approx 77.6$. In the large texture, the decomposed signals of q'' and $\tilde{q}$ show that the coherent part, $\tilde{q}$, is the major contribution to the near wall increase of the turbulence intensity. The homogenized slip length simulation, H26, can approximately capture the behavior of q'' in RP26, while non-negligible deviations are observed. In figure 7 we show coherent flow structures for a unit pattern. As indicated by [27], figure 7(a) and (b) demonstrate the stagnation of slipping flow. A counter-rotating streamwise vortex pair is induced on top of a post shown in (b), as previously reported in studies for streamwise ridges [23–26]. As we shall see, the effect

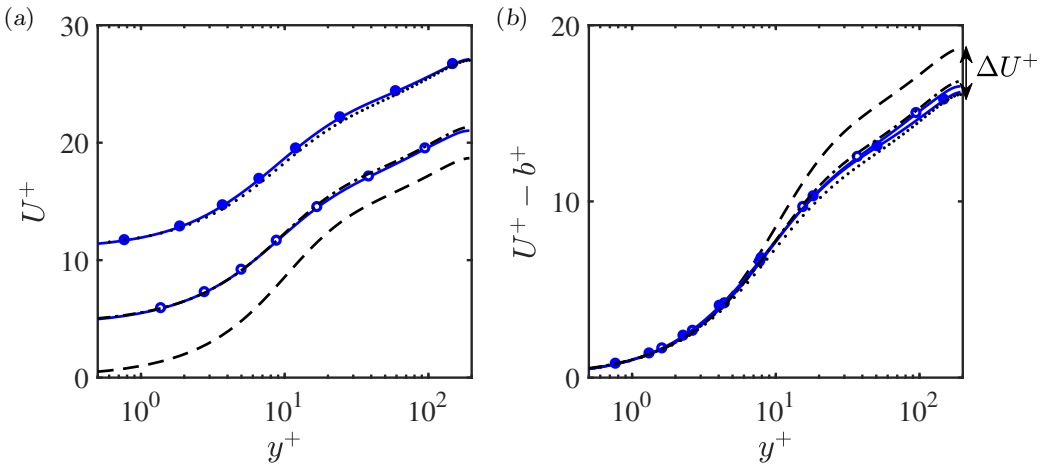

Figure 5. Mean velocity profiles (a) U^+ and (b) $U^+ - b^+$ for $\phi_s = 1/9$, -○-, Patterned slip with randomly distributed posts, $R04_1$; -●-, Patterned slip, $R26_1$; - · - · -: Homogenized slip using the slip length from H04, ·····: Homogenized slip H26. – – – –: smooth-wall.

of these coherent structure on the momentum transport is small because the magnitude of the coherent structure is small and not as significant as what has been observed in the case of streamwise ridges [25, 26].

Total shear stress, $\tau^+_{xy,tot}$, budgets are plotted in figure 8. The total shear stress is decomposed into the viscous shear stress, $\tau^+_{xy,v} = d\overline{U}^+/dy^+$, Reynolds stress by random part $\tau^+_{xy,R} = -\overline{u''v''}^+$, Reynolds stress by coherent part, $\tau^+_{xy,c} = -\overline{\tilde{u}\tilde{v}}^+$. In the small texture size, $L_n^+ \approx 12.9$, the magnitude of Reynolds stress is larger than that of smooth wall in the buffer layer ($5 \lessapprox y^+ \lessapprox 30$) and the viscous stress is compensated due to the increase of Reynolds shear stress. The homogenized slip length simulation matches the Reynolds stress budget of randomly distributed posts. In the large texture size $L_n^+ \approx 77.4$, the Reynolds stress by coherent part is augmented compared to the smaller texture, however, its contribution to the total Reynolds shear stress remains small. This suggests that the shortening of buffer layer in the mean velocity profile of randomly distributed posts is mainly caused by slippage effects, not mainly by the coherent secondary flows.

C. Pressure fluctuation and interfacial robustness

Next, we investigate the effect of geometric randomness on the interfacial robustness of the gas-liquid interface by investigating wall pressure fluctuations and reconstructed interface deformations. Figure 9 shows instantaneous wall pressure fluctuations for periodically aligned posts and randomly distributed posts. For both cases, we found that pressure signals show two distinct features: a time-fluctuating signal due to the time variation of the overlying turbulence (q'') and a time-independent signal associated with stagnation of the slipping flow near the leading edge of the posts ($\tilde{q}$). In smaller texture size, the turbulence contribution dominates and the pressure fluctuation is similar to the smooth wall. In large texture size limit, $L^+ \approx 77.6$ the dominant pressure fluctuation is the stagnation pressure. The irregular clustering of the posts results in variations of stagnation pressure, while the spatial variations of stagnation pressure in the aligned posts is mainly due to its time-dependent components.

The root-mean-square (rms) wall pressure fluctuations of the randomly distributed post, $\tilde{p}^+_{rms_0}$, is found to be close to that of the aligned post cases as shown in figure 10(a). When we consider $\tilde{p}^+_{rms_0}$ against slip velocity, U_s^+, as shown in figure 10(b), however, the wall stagnation pressure fluctuation of the randomly distributed posts is larger than that of the aligned posts at a given slip velocity due to about 30% reduction of slip length at the same nominal texture size. The wall stagnation pressure fluctuation increases linearly with increasing slip velocity as

$$\tilde{p}^+_{rms_0} \approx 0.48 U_s^+ + 0.79. \tag{6}$$

The ensemble averaged wall stagnation pressure distribution, over Voronoi cells, is found to be self-similar when distance is scaled with w^+ and the stagnation pressure is scaled with $\tilde{p}_{rms_0}$ as shown in figure 10(c).

More detailed analysis on the deformation of the interface reveals that the randomness of the textures decreases the stability of gas-liquid interface. From time-averaged wall pressure fields, we obtain interface deformation by solving the Young-Laplace equation, Eq. (4). We analyze the interface stability in terms of maximum interface deformation for each individual post in different locations. The maximum deformation angle occurs at the leading edge of posts

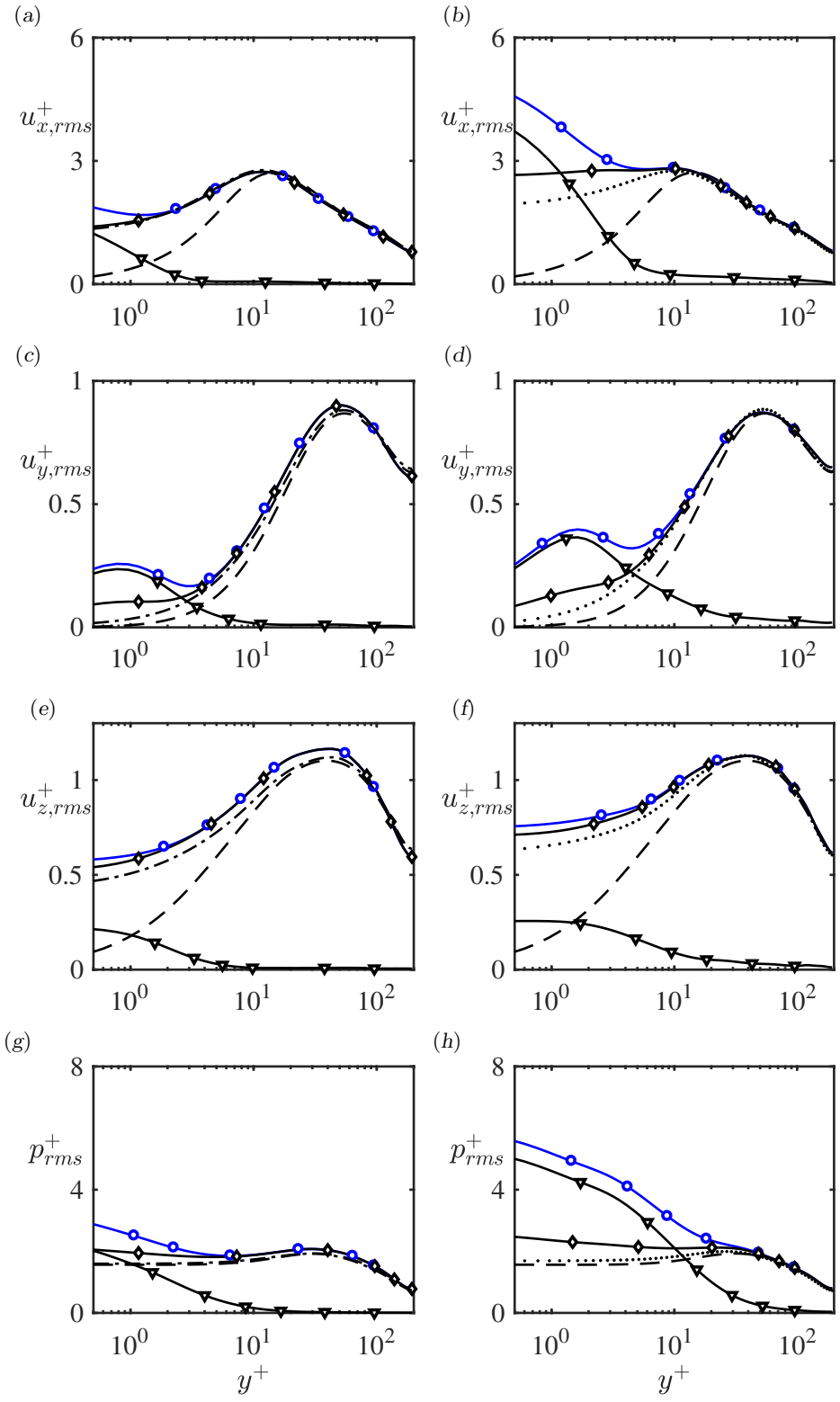

Figure 6. (a) Streamwise, (c) wall-normal, (e) spanwise, (f) pressure rms fluctuations for R04 with $L_n^+ \approx 12.9$. (b) u_x, (d) u_y, (f) u_z, (d) p, for R26 with $L_n^+ \approx 77.4$. -○-: q'_{rms}, -◇-: q''^+_{rms}, -▽-: $\tilde{q}^+_{rms}$, Homogenized slip, - · - · -: H04, ·····: H26. – – – –: smooth-wall.

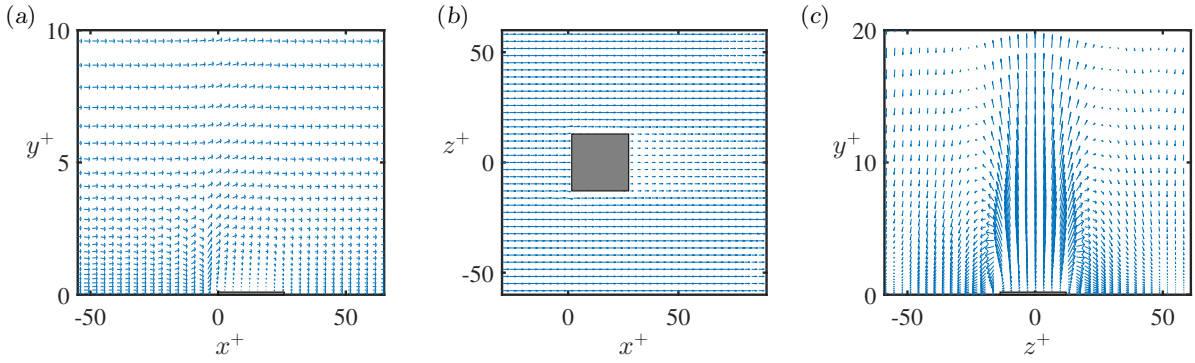

Figure 7. Coherent secondary flow structure near the post with $w^+ \approx 26$: (a) vector plots of $\tilde{u}_y$ and $U + \tilde{u}_x$ in $x - y$ plane, (b) velocity contours of $U + \tilde{u}_x$ and $\tilde{u}_z$ in $x - z$ plane (c) velocity contours of $\tilde{u}_y$ and $\tilde{u}_z$ in $y - z$ plane. The location of post is indicated by gray boxes.

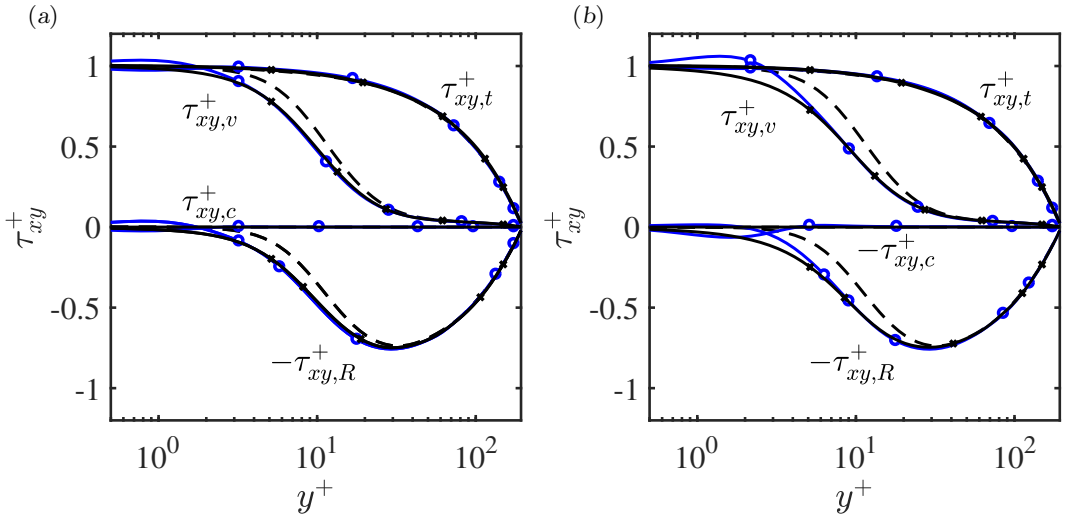

Figure 8. Shear stress budget in wall normal direction. (a) $L_n^+ \approx 12.9$, -O-: Randomly distributed posts, R04, -×-, homogenized slip, HP04 (b) $L_n^+ \approx 77.4$, -O-: Randomly distributed posts, R26, -×-, homogenized slip, HP26, - - - -: smooth-wall. $\tau^+_{xy,v}$ is viscous shear stress, $d\overline{U}^+/dy^+$, $\tau^+_{xy,R}$ is Reynolds stress, $-\overline{u''v''}^+$, $\tau^+_{xy,c}$ is Reynolds stress from coherent fluctuation, $-\overline{\tilde{u}\tilde{v}}^+$, and $\tau^+_{xy,tot}$ is total shear stress, $\tau^+_{xy,tot} = \tau^+_{xy,R} + \tau^+_{xy,v} + \tau^+_{xy,c}$.

facing upstream slipping flow. The contact angle at the leading edge is defined as $\theta_L = \frac{\pi}{2} + \tan^{-1}(d\eta/dx|_L)$, where $(d\eta/dx)_L$ is the slope of the interface profile at the leading edge [27]. The onset of interface breakage can be triggered when the large deformation angle of interface exceeds the advancing contact angle that can be achievable only with chemical coating, $\theta_L \gtrapprox 120°$. In figure 11, the deformation angles are reported for each randomly distributed post. Due to randomness in the pattern, the deformation angle for each post is different depending on the arrangement of the texture. The maximum deformation angle is more than twice that of aligned posts at matched $L_n^+ \approx 77$ as shown in figure 11(a). For smaller texture size $L_n^+ \approx 26$, the maximum deformation angle is 2.6 times that of aligned posts. The distributions of deformation angles plotted in the inset of figure 11 show that the peak of the distribution is near the mean, and the mean of deformation angle for randomly distributed posts is close to that of aligned posts. Throughout all texture sizes, $L_n^+ \approx 13 - 77$, the maximum deformation angles of randomly distributed posts are plotted in figure 12(a). The maximum deformations of SHS with randomly distributed textures are more than twice that of the periodically aligned post cases.

Based on our findings, we provide the critical texture size that limits the stable operation of SHSs in turbulent flows in figure 12(b). Due to the increases maximum deformation, the critical texture size of SHS with randomly distributed textures is less than that of aligned posts. The maximum allowed L^+ is reduced by factor of ≈ 0.5, compared to aligned case for $We^+ = 10^{-3} - 10^{-2}$.

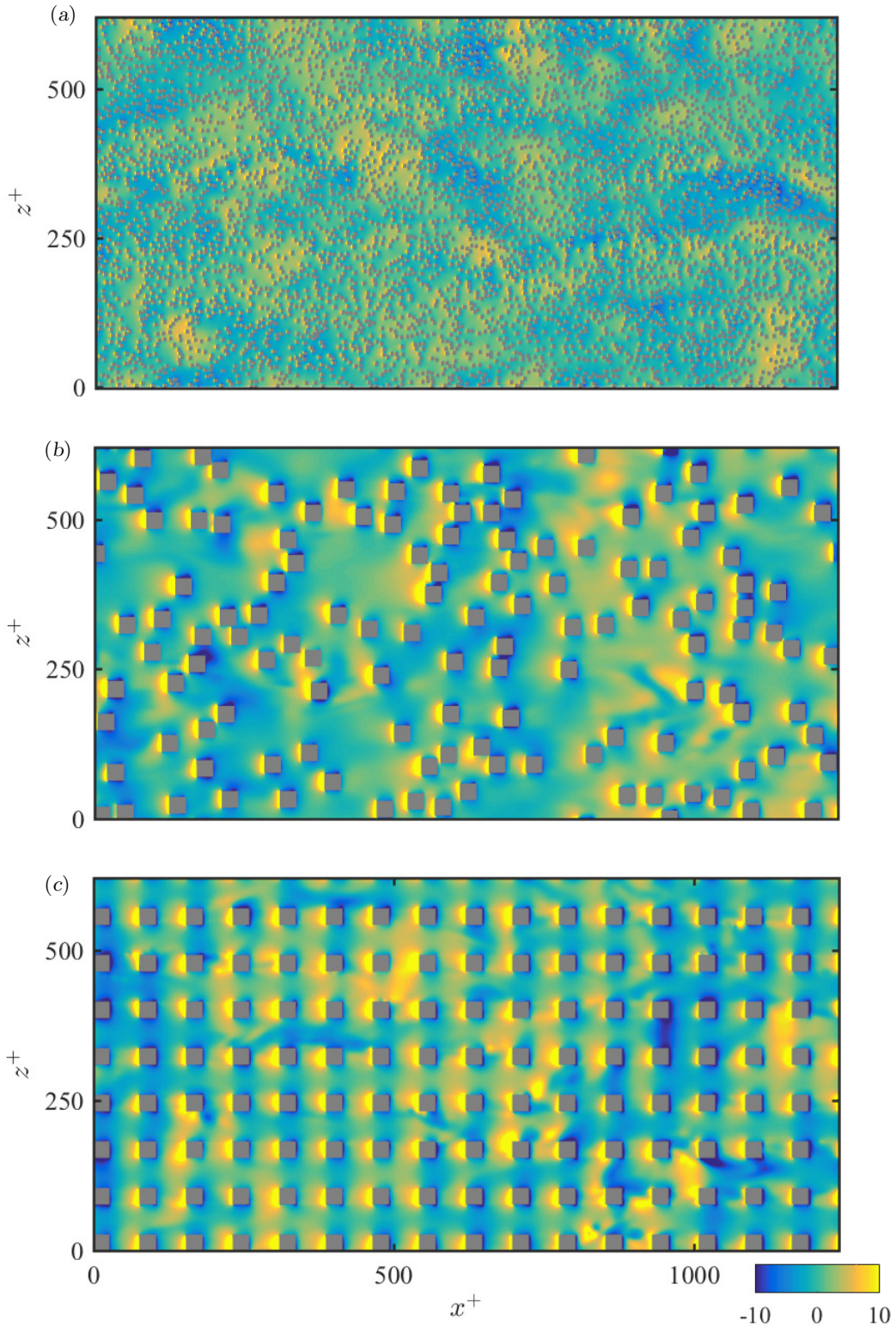

Figure 9. Instantaneous wall pressure snapshots, $p_0'^+ = p_0'/(\rho u_\tau^2)$, on superhydrophobic surfaces for (a) randomly distributed posts, R04$_1$, $L_n^+ \approx 13$, (b) randomly distributed posts, R26$_1$, $L_n^+ \approx 77$, (c) aligned posts, $L_n^+ \approx 77$. From blue to yellow, color shows pressure fluctuations from -10 to 10.

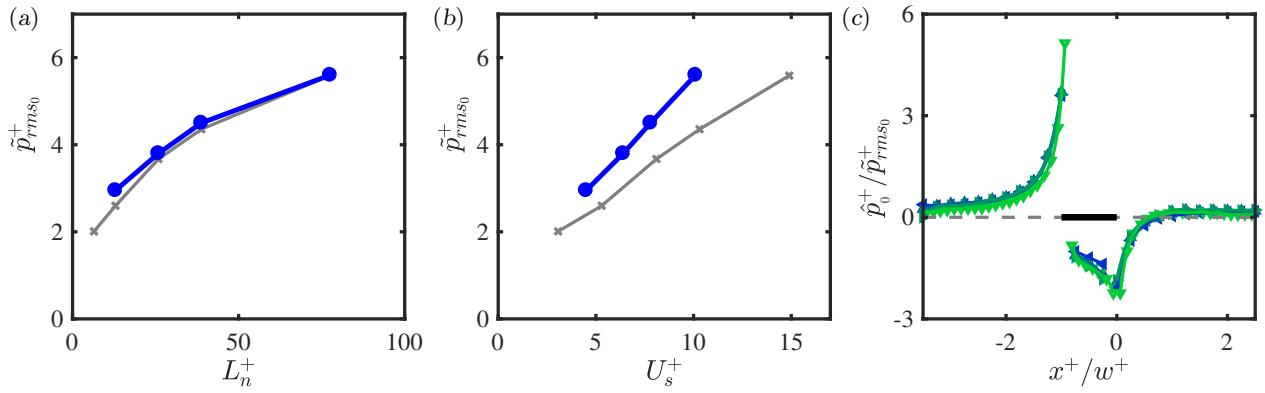

Figure 10. (*a*) Wall rms pressure fluctuation due to stagnation, $\tilde{p}^+_{rms_0}$ against nominal texture size L_n^+; (*b*) $\tilde{p}^+_{rms_0}$ versus slip velocity U_s^+. –●–: randomly distributed posts; –×–: aligned posts. (*c*) Self-similar profiles of wall pressure distribution due to stagnation on the gas-liquid interface. The plots show pressure profiles on the centerline going through the middle of post width. $L_n^+ \approx 13$; –▲–: $L_n^+ \approx 26$; –►–: $L_n^+ \approx 38$; –▼–: $L_n^+ \approx 77$.

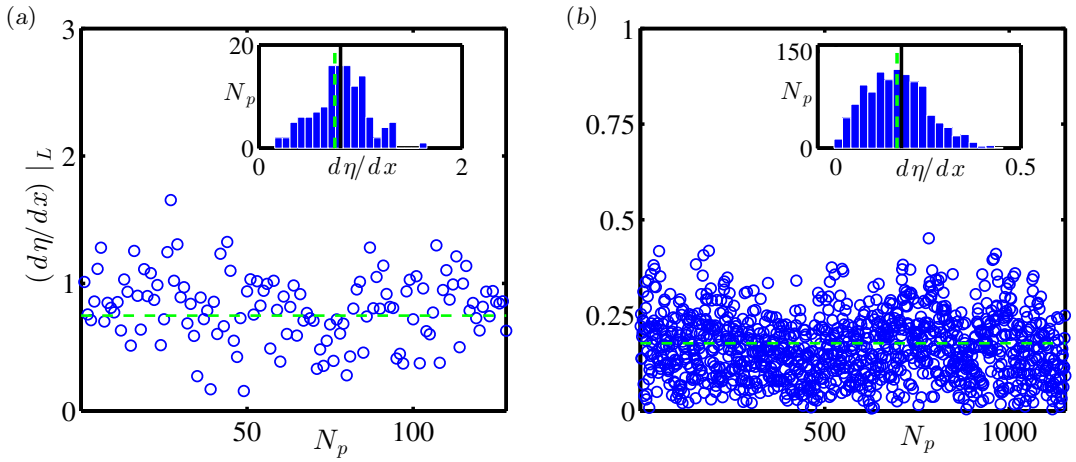

Figure 11. Interface deformation angle, $(d\eta/dx|_L)$, due to stagnation pressure for randomly distributed posts versus number of posts, N_p, as compared to aligned posts with Weber number $We^+ = 5 \times 10^{-3}$ for texture size (a) $L_n^+ \approx 77$; (*b*) $L_n^+ \approx 26$. ○: Randomly distributed posts; Insets: histogram of interface deformation angle due to stagnation pressure for randomly distributed posts versus number of posts. ——: mean of $(d\eta/dx|_L)$ of randomly distributed posts; – – – –: $(d\eta/dx|_L)$ of aligned posts.

IV. SUMMARY

The present work studied the effects of randomness of the SHS texture distribution on hydrodynamic performance when exposed to an overlaying turbulent flow. We conduct direct numerical simulations of turbulent flows over randomly patterned interfaces, considering texture size $w^+ \approx 4 - 26$, and solid fractions, $\phi_s = 11 - 25\%$. Patterned slip and no-slip boundary conditions are imposed on channel walls modeling the entrapped gas within the SHS roughness. The slip length of random textures matches with a linear prediction from Stokes solution in the limit of small texture size, $w^+ \approx 4$. For larger textures this linear growth slows down in a fashion similar to previous observations in aligned textures. In the small texture size limit, the solid fraction dependency of the slip length from the DNS data indicates a good agreement with the trends suggested by the Stokes flow solutions. The slip length of random textures is found to be about 30% less than that of aligned textures keeping Re_τ, w^+, and ϕ_s the same. Statistics of fluctuations are obtained and decomposed into coherent and random components, induced by geometry and turbulence respectively. The homogenized isotropic slip length model accurately predict the increase of turbulence intensities as well as Reynold shear stresses of SHS of randomly distributed posts with small texture size, while missing the coherent components due to geometry. The turbulence intensities of SHS with randomly distributed posts deviate from the homogenized model, as texture size becomes larger. The homogenized slip length model also accurately predicts the momentum deficit due to shortening of buffer layer in the mean velocity profile for entire

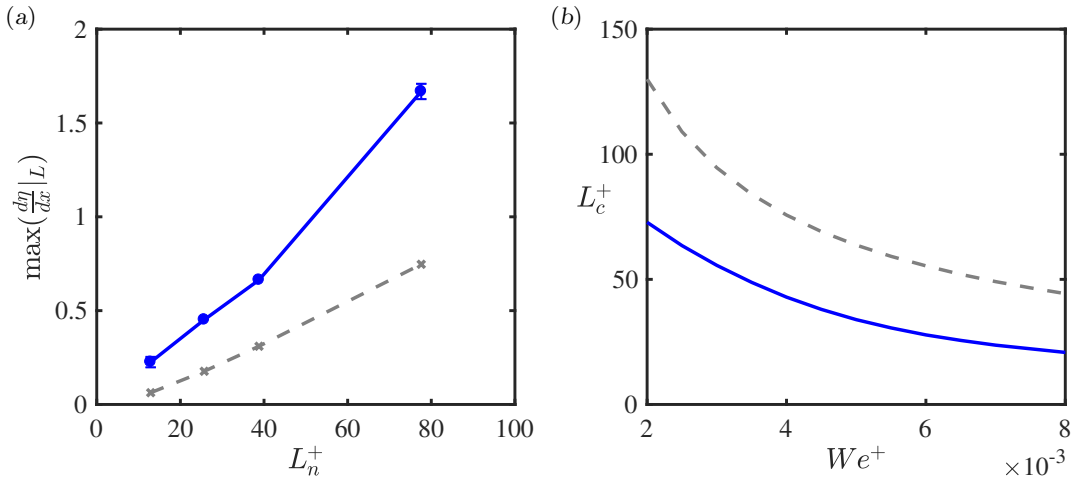

Figure 12. (a) Comparison of maximum interface deformation slope, max $(d\eta/dx)|_L$, due to stagnation pressure for randomly distributed posts and aligned posts versus effective texture size, $L_n^+ = w^+/\sqrt{\phi_s}$, at Weber number $We^+ = 5 \times 10^{-3}$. –●–: randomly distributed posts; –×–: aligned posts [27]. For $L_n^+ \approx 13$ and $L_n^+ \approx 77$, error bars are plotted by taking account for different texture arrangements. (b) The critical texture size, L_c^+, is plotted against We^+ when $\theta_{adv} = 120°$. ——: current study, - - - -: aligned posts.

range of texture size considered in this study, as opposed to aligned texture cases, that showed discrepancies in large texture sizes. We show that for fixed texture size, solid fraction, and wall friction, the randomness of the feature distribution decreases the stability of the gas pocket as compared to surfaces with aligned features. The rms wall pressure fluctuation of randomly distributed posts is close to that of aligned posts for fixed wall shear. When plotted against the slip length, the pressure fluctuations of the random surface is larger than that for a surface with aligned textures. The deformation of the gas-liquid interface is obtained through Young-Laplace equation and the interfacial stability is assessed using the maximum deformation angle at the leading edge of the posts. The detailed analysis on the maximum deformation of individual post sites shows that the randomness of texture arrangement increases the possibility of interface breakage as compared to the aligned case, this is because, at worst, the post encounters interface deformation angles at least twice as large as those in the case of aligned posts.

ACKNOWLEDGMENTS

This work was supported by the Office of Naval Research under grant No. 3002451214. The authors greatly appreciate the Kwanjeong Educational Foundation for the funding support for Jongmin Seo.

[1] J. P. Rothstein. Slip on superhydrophobic surfaces. *Annu. Rev. Fluid Mech.*, 42:89–109, 2010.
[2] K. B. Golovin, J. W. Gose, M. Perlin, S. L. Ceccio, and A. Tuteja. Bioinspired surfaces for turbulent drag reduction. *Phil. Trans. R. Soc. A*, 374:20160189, 2016.
[3] J. Ou, J. B. Perot, and J. P. Rothstein. Laminar drag reduction in microchannels using ultrahydrophobic surfaces. *Phys. Fluids*, 16:4635–4643, 2004.
[4] J. Lauga and H. Stone. Effective slip in pressure-driven stokes flow. *J. Fluid Mech.*, 489:55–77, 2003.
[5] C. Ybert, C. Barentin, and C. Cottin-Bizonne. Achieving large slip with superhydrophobic surfaces: Scaling laws for generic geometries. *Phys. Fluids*, 19:123601, 2007.
[6] A. M. J. Davis and E. Lauga. Hydrodynamic friction of fakir-like superhydrophobic surfaces. *J. Fluid Mech.*, 661:402–411, 2010.
[7] C. Lee, C. Choi, and C.-J. Kim. Structured surfaces for a giant liquid slip. *Phys. Rev. Lett.*, 101:064501, 2008.
[8] J. S. Wexler, I. Jacobi, and H. A. Stone. Shear-driven failure of liquid-infused surfaces. *Phys. Rev. Lett.*, 114:168301, 2015.
[9] Y. Liu, J. S. Wexler, C. Schönecker, and H. A. Stone. Effect of viscosity ratio on the shear-driven failure of liquid-infused surfaces. *Phys. Rev. Fluids*, 1:074003, 2016.
[10] J. S. Wexler, A. Grosskopf, M. Chow, Y. Fan, I. Jacobi, and H. A. Stone. Robust liquid-infused surfaces through patterned wettability. *Soft Matter*, 11:5023–5029, 2015.

[11] R. Daniello, N. E. Waterhouse, and J. P. Rothstein. Turbulent drag reduction using superhydrophobic surfaces. *Phys. Fluids*, 21:085103, 2009.

[12] H. Park, G. Sun, and C.-J. Kim. Superhydrophobic turbulent drag reduction as a function of surface grating parameters. *J. Fluid Mech.*, 747:722–734, 2014.

[13] R. A. Bidkar, L. Leblanc, A. J. Kulkarni, V. Bahadur, S. L. Ceccio, and M. Perlin. Skin-friction drag reduction in the turbulent regime using random-textured hydrophobic surfaces. *Phys. Fluids*, 26:085108, 2014.

[14] S. Srinivasan, J. A. Kleingartner, J. B. Gilbert, R. E. Cohen, A. J. B. Milne, and G. H. McKinley. Sustainable drag reduction in turbulent taylor-couette flows by depositing sprayable superhydrophobic surfaces. *Phys. Rev. Lett.*, 114:014501, 2015.

[15] H. Ling, S. Srinivasan, K. Golovin, A. Tuteja G. H. McKinley, and J. Katz. High-resolution velocity measurement in the inner part of turbulent boundary layers over super-hydrophobic surfaces. *J. Fluid Mech.*, 801:670–703, 2016.

[16] H. Ling, J. Katz, M. Fu, and M. Hultmark. Effect of reynolds number and saturation level on gas diffusion in and out of a superhydrophobic surface. *Phys. Rev. Fluids*, 2:124005, 2017.

[17] T. Min and J. Kim. Effects of hydrophobic surface on skin-friction drag. *Phys. Fluids*, 16:L55–L58, 2004.

[18] K. Fukagata, N. Kasagi, and P. Koumoutsakos. A theoretical prediction of friction drag reduction in turbulent flow by superhydrophobic surfaces. *Phys. Fluids*, 18:051703, 2006.

[19] A. Busse and N. D. Sandham. Influence of an anisotropic slip-length boundary condition on turbulent channel flow. *Phys. Fluids*, 24:055111, 2012.

[20] T. Jung, H. Choi, and J. Kim. Effects of the air layer of an idealized superhydrophobic surface on the slip length and skin-friction drag. *J. Fluid Mech.*, 790:R1, 2016.

[21] M. B. Martell, J. B. Perot, and J. P. Rothstein. Direct numerical simulations of turbulent flows over superhydrophobic surfaces. *J. Fluid Mech.*, 620:31–41, 2009.

[22] H. Park, H. Park, and J. Kim. A numerical study of the effects of superhydrophobic surface on skin-friction drag in turbulent channel flow. *Phys. Fluids*, 25:110815, 2013.

[23] T. O. Jelly, S. Y. Jung, and T. A. Zaki. Turbulence and skin friction modification in channel flow with streamwise-aligned superhydrophobic surface texture. *Phys. Fluids*, 26(095102), 2014.

[24] J. Lee, T. O. Jelly, and T. A. Zaki. Effect of reynolds number on turbulent drag reduction by superhydrophobic surface textures. *Flow Turbulence Combustion*, 95:277–300, October 2015.

[25] S. Türk, G. Daschiel, A. Stroh, Y. Hasegawa, and B. Frohnapfel. Turbulent flow over superhydrophobic surfaces with streamwise grooves. *J. Fluid Mech.*, 747:186–217, 2014.

[26] A. Rastegari and R. Akhavan. On the mechanism of turbulent drag reduction with super-hydrophobic surfaces. *J. Fluid Mech.*, 773:R4, 2015.

[27] J. Seo, R. García-Mayoral, and A. Mani. Pressure fluctuations and interfacial robustness in turbulent flows over superhydrophobic surfaces. *J. Fluid Mech.*, 783:448–473, 2015.

[28] J. Seo and A. Mani. On the scaling of the slip velocity in turbulent flows over superhydrophobic surfaces. *Phys. Fluids*, 28:025110, 2016.

[29] Hyung Jae Im and Jae Hwa Lee. Comparison of superhydrophobic drag reduction between turbulent pipe and channel flows. *Phys. Fluids*, 29:095101, 2017.

[30] A. Rastegari and R. Akhavan. The common mechanism of turbulent skin-friction drag reduction with superhydrophobic longitudinal microgrooves and riblets. *J. Fluid Mech.*, 838:68–104, 2018.

[31] M. K. Fu, I. Arenas, S. Leonardi, and M. Hultmark. Liquid-infused surfaces as a passive method of turbulent drag reduction. *J. Fluid Mech.*, 824:688–700, 2017.

[32] J. Seo, R. García-Mayoral, and A. Mani. Turbulent flows over superhydrophobic surfaces: flow-induced capillary waves, and robustness of air-water interfaces. *J. Fluid Mech.*, 835:45–85, 2018.

[33] L. Piao and H. Park. Two-dimensional analysis of air-water interface on superhydrophobic grooves under fluctuating water pressure. *Langmuir*, 31:8022–8032, 2015.

[34] E. Aljallis, M. A. Sarshar, R. Datla, V. Sikka, and A. Jone. Experimental study of skin friction drag reduction on superhydrophobic flat plates in high Reynolds number boundary layer flow. *Phys. Fluids*, 25:025103, 2013.

[35] H. Haibao, D. Peng, Z. Feng, S. Dong, and W. Yang. Effect of hydrophobicity on turbulent boundary layer under water. *Experimental Thermal and Fluid Science*, 60:148–156, 2015.

[36] J. Zhang, H. Tian, Z. Yao, P. Hao, and N. Jiang. Mechanisms of drag reduction of superhydrophobic surfaces in a turbulent boundary layer flow. *Exp. in Fluids*, 56:179, 2015.

[37] B. Vajdi Hokmabad and S. Ghaemi. Turbulent flow over wetted and non-wetted superhydrophobic counterparts with random structure. *Phys. Fluids*, 28:015112, 2016.

[38] M. Sbragaglia and A. Prosperetti. Effective velocity boundary condition at a mixed slip surface. *J. Fluid Mech.*, 578:435–451, 2007.

[39] M. A. Samaha, T. H. Vahedi, and M. Gad el Hak. Modeling drag reduction and meniscus stability of superhydrophobic surface of random roughness. *Phys. Fluids*, 23:012001, 2011.

[40] Karim Alame and Krishnan Mahesh. Wall-bounded flow over a realistically rough superhydrophobic surface. *arXiv:1802.06845v1 [physics.flu-dyn]*, 2018.

[41] C. Schönecker, T. Baier, and S. Hardt. Influence of the enclosed fluid on the flow over a microstructured surface in the cassie state. *J. Fluid Mech.*, 740:168–195, 2014.

[42] J. Kim and P. Moin. Application of a fractional step method to incompressible Navier-Stokes equations. *J. Comput. Phys.*, 59:308–323, 1985.